27 May 2010, 7:30 pm - 9:00 pm

Displacement Ductility Capacity of Fixed-Head Piles

Jiunn-Shyang Chiou
National Center for Research on Earthquake Engineering, Taiwan

Cheng-Hsing Chen
National Taiwan University, Taiwan


Fifth International Conference on
Recent Advances in Geotechnical Earthquake Engineering and Soil Dynamics
and Symposium in Honor of Professor I.M. Idriss
May 24-29, 2010 • San Diego, California

DISPLACEMENT DUCTILITY CAPACITY OF FIXED-HEAD PILES

Jiunn-Shyang Chiou
National Center for Research on Earthquake Engineering
Taipei, Taiwan, R.O.C. 10668

Cheng-Hsing Chen
Department of Civil Engineering, National Taiwan University
Taipei, Taiwan, R.O.C. 10617

ABSTRACT

This study performs a parametric study on the displacement ductility capacity of a fixed-head pile. The Winkler-beam model is employed, in which both the soil nonlinearity and pile nonlinearity are adequately considered. In this parametric study, the pile is regarded as a limited ductility structure which conditionally allows the pile deformation to enter the plastic range during loadings. The analysis variables include the axial force, the pile diameter, the longitudinal reinforcement ratio, and the soil stiffness. The relationships of the displacement ductility capacity of the pile to the curvature ductility capacity and to the over-strength ratio of the pile section are examined through a large number of pushover analyses. Results show that the axial force level, the pile diameter, and the steel ratio remarkably influence the displacement ductility capacity of a fixed-head pile. Their influence can be represented mainly by the over-strength ratio of the pile section. Besides, the influence of the soil stiffness is insignificant: the displacement ductility capacity slightly decreases with the soil stiffness.

INTRODUCTION

In designing a pile in seismic design, it is preferable to design the pile as an elastic structure. However, considering the occurrence of severe earthquakes, it will become impractical to design the piles to remain in the elastic stage, especially for a fixed-head pile. The head of the fixed-head pile usually experiences a larger curvature when the pile cap is subjected to a lateral displacement. It will be cost-effective to allow the piles to deform into the plastic range for energy dissipation. Thus, the ductility capacity of piles is important in the seismic design.

Budek et al. (2000) adopted the Winkler-beam model to conduct parametric analyses for the displacement ductility capacity of RC pile/columns in granular soils. Their study used the pile-head height above the ground surface and the soil stiffness as variables, but did not consider the influence of structural properties of the pile/columns. Song et al. (2005) applied a concentrated plastic-hinge model to investigate the relationship between the displacement ductility of fixed-head piles and the curvature ductility of the pile section. However, the concentrated hinge model is actually unable to simulate the spread of plasticity along the pile shaft since the range of plasticity is specified beforehand in the model and stays constant in the whole analysis process (Chiou, et al 2009).

To identify the major influencing factor on the ductility capacity of a fixed-head pile clearly, this study conducts parametric analyses. The parametric analyses consider the influences of the axial force level, the pile diameter, the longitudinal reinforcement ratio, and the soil stiffness.

PUSHOVER MODEL

This study adopts the Winkler-beam model to build a pushover model for the parametric analyses, in which the pile is modeled as a beam and the soil reactions are simulated by using spring elements.

To model the pile nonlinearity, the distributed plastic hinge model is used. As shown in Fig. 1, the model is to pre-set a series of plastic hinges distributed over a range where the plasticity may develop. Once the moments at the assigned hinges exceed the yield moment of the pile section, the hinges will produce plastic rotations. The active hinges thus define an actual plastic zone. The procedure to determine the property of the distributed plastic hinges can refer to Chiou, et al. (2009), which is based on the moment-curvature relation of the pile section. Unlike the concentrated plastic hinge model, this distributed plastic hinge model is unnecessary to pre-set the plastic-hinge length for a plastic hinge and can model the plasticity propagation in the pile.

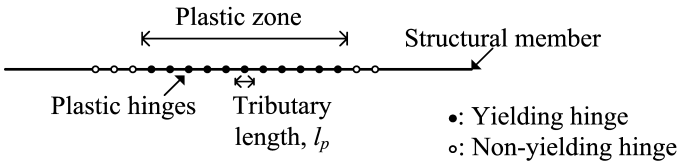

Fig. 1. Distributed plastic hinge model (Chiou, et al. 2009)

The soil spring model uses a nonlinear *p-y* curve to consider soil nonlinearity, in which *p* is the soil reaction and *y* is the lateral displacement of the soil. The nonlinear *p-y* curve adopted in this study is shown in Fig. 2, which is defined as

$$p = k_h \cdot D \cdot y \tag{1}$$

where k_h is the subgrade reaction coefficient at the lateral displacement *y* and *D* is the pile diameter. In this study, the subgrade reaction coefficient k_h follows the recommendations proposed by the Architecture Institute of Japan (1988), as follows.

The yield displacement y_y of the *p-y* curve is generally set to 0.01m. The initial subgrade reaction coefficient k_{h0} at the linear part of the *p-y* curve is given as:

$$k_{h0} = 80 \cdot E_0 \cdot D^{-0.75} \tag{2}$$

where k_{h0} (MN/m^3) is the initial subgrade reaction coefficient; E_0 is the soil modulus, which can be estimated from an empirical equation as E_0=0.7*N* (MN/m^2), in which *N* is the blow number of Standard Penetration Test; *D* is the pile diameter in centimeter.

For the nonlinear part that *y* is beyond y_y, the following relation is applied;

$$k_h = k_{h0} \cdot (y / y_y)^{-0.5} \tag{3}$$

where k_h is the subgrade reaction coefficient when the lateral displacement *y* (m) is beyond y_y (m).

For the ultimate part, it is assumed that the soil reaction reaches its ultimate pressure when the lateral displacement is one-tenth of the pile diameter (*D*/10).

PRARMETRIC STUDIES

In the parametric study, a fixed-head reinforced concrete pile with a length of 25 m embedded in uniform soils is adopted as shown in Fig. 3. The compressive strength of concrete f_c' is 28 MPa. The yield strength of rebar f_y is 414 MPa. The concrete cover is set to be 0.075 m. The transverse steel ratio ρ_t is set to be 1%.

The parameters adopted are listed in Table 1. The axial force level is represented by $P/(f_c'A_g)$, where *P* is the axial force, f_c' is the compressive strength of concrete, and A_g is the gross area of the pile section. The pile diameter is represented by *D*. The longitudinal reinforcement ratio is represented by ρ_l. The soil stiffness is represented by the SPT-N value (*i.e.*, the blow number of Standard Penetration Test). This study performs a total of 64 cases for the parametric values.

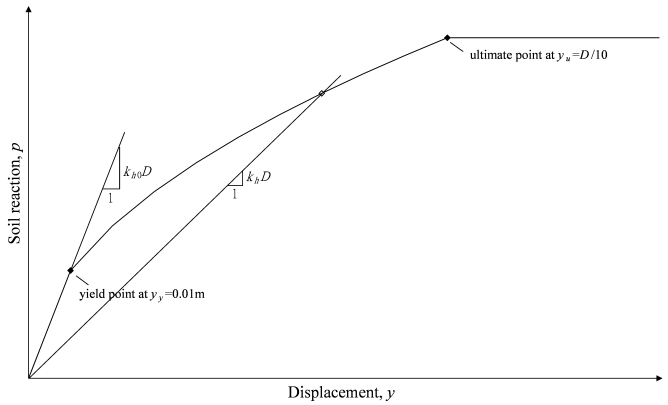

Fig. 2 P-y model for nonlinear Winkler springs

Moment-Curvature Relations

All variables, except for the SPT-N value, considered above will change the sectional property of the pile.

Treating the pile as a limited ductility structure, this study sets the ultimate state of the pile section to be a limit state of damage control. The "damage-control" implies that only repairable damage occurs. According to Kowalsky (2000), the tension strain limit of the steel and the compression strain limit of the core concrete are set to 0.06 and 0.018, respectively. According to the aforementioned limit strains and nonlinear stress-strain relations of steel and concrete, the moment-curvature relation of a reinforced concrete pile section under combined axial load and flexure can be obtained through section analyses. For the stress-strain relationship of concrete, the cover concrete is simulated by the general unconfined concrete model and the core concrete is modeled by the confined concrete model proposed by Mander et al. (1988) for the confined effects of stirrups. For the stress-strain relationship of reinforcing steel, the steel model considering the hardening behavior of steel is employed.

Generally, a typical nonlinear moment-curvature relation of a pile section can be calculated as shown in Fig. 4 (the dashed line). For easy modeling, the nonlinear moment-curvature curve can usually be simplified as a bilinear curve by applying the equal-energy rule. As shown in Fig. 4, the position of an effective yield point can thus be determined by equating the areas under the bilinear curve (solid line) and the original nonlinear moment-curvature curve (dashed line). Based on the bilinear moment-curvature relationship, two parameters

including the curvature ductility capacity μ_ϕ and the sectional over-strength ratio ω can be defined to describe the nonlinear characters of the pile section:

$$\mu_\phi = \phi_u / \phi_y \tag{4}$$

$$\omega = M_u / M_y \tag{5}$$

where ϕ_u is the ultimate curvature; ϕ_y is the effective yield curvature; M_u is the ultimate moment, and M_y is the effective yield moment.

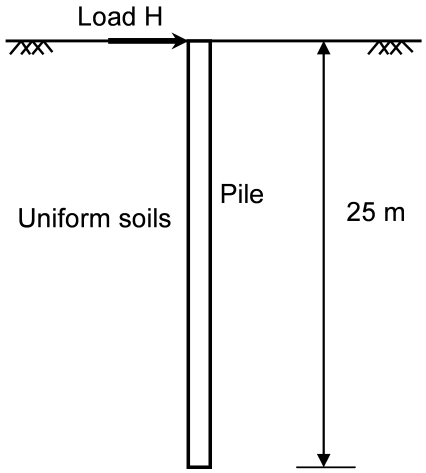

Fig. 3. Pile-soil model for parametric studies

Table 1 Parametric cases

Parameter	Value
Axial force level, $P/(f_c'A_g)$	-0.1, 0.0, 0.1, 0.2 (positive for compression; negative for tension)
Pile diameter, D (m)	1.0, 1.5
Longitudinal steel ratio, ρ_l (%)	1, 2
SPT-N values	5, 10, 20, 30

In these two parameters, the curvature ductility capacity μ_ϕ has been thought as an important factor that can be directly related to the ductility capacity of a column or a pile (Kowalsky 2000; Chai 2002; Song et al. 2005). However, this study attempts to investigate the significance of the sectional over-strength ratio to the ductility capacity of a member.

Fig. 5 shows the moment-curvature relations for the pile sections of D=1m and ρ_l=1% that are subjected to the various axial load levels. The initial stiffness and the strength of the pile section increase with the axial compression force level. The yield curvatures of these sections are quite close. The ultimate curvature decreases as the axial compression force level increases or decreases from zero. The curvature ductility capacities of the pile sections shown in Fig. 5 are quite close, about 17-20. When the axial force level is zero, the curvature ductility capacity is the largest. In other words, when the axial compression force increases or decreases from zero, the curvature ductility capacity decreases. In Fig. 5, it can also be seen that the sectional over-strength ratio decreases as the axial compression force increases; the section with tension has the largest over-strength ratio.

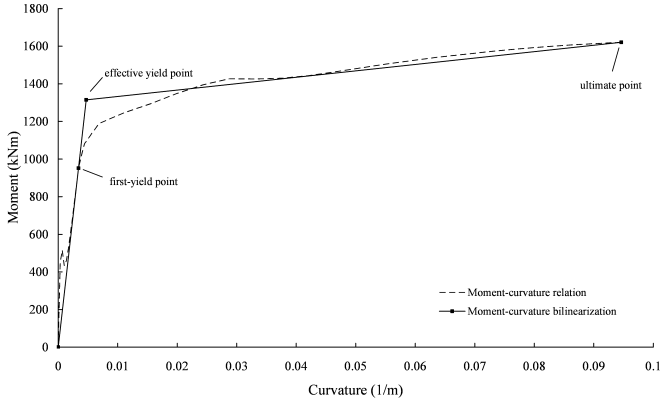

Fig. 4 Bilinearization of moment-curvature curve

Fig. 6 presents the moment-curvature relations for the pile sections with ρ_l=1% and $P/(f_c'A_g)$=0 for D=1m and 1.5m. The stiffness and the strength of the pile section increase with the pile diameter. The yield and ultimate curvatures decrease with the pile diameter, which is due to the larger neutral-axial depth for D=1.5m. In Fig. 7, it can be seen that the curvature ductility capacity for D=1m (20.1) is a little higher than that for D=1.5m (18.4). However, it is not always true when comparing all the cases with D=1m and D=1.5m. Because both the yield and the ultimate curvatures decrease with the pile diameter, the resulting curvature ductility capacity does not monotonically vary with the pile diameter. On the other hand, it can be found that the over-strength ratio will increase with the pile diameter.

Figure 7 depicts the moment-curvature relations for the pile sections with D=1m and $P/(f_c'A_g)$=0 for ρ_l=1% and 2%. The section with the higher steel ratio exhibits higher stiffness and ultimate strength. Their yield curvatures are close; however, the ultimate curvature is smaller when the steel ratio is higher so that the curvature ductility capacity for ρ_l=2% (18.18) is lower than that for ρ_l=1% (20.1). As for the sectional over-strength ratio, the over-strength ratio increases as the steel ratio increases.

Summarizing the results of all the cases, it can be found that the curvature ductility capacities obtained are quite large, implying that the pile sections exhibit sufficient ductility. It can also be found that the sectional over-strength ratio values depend on the axial force level, the pile diameter, and the steel ratio. For the cases with $P/(f_c'A_g) \geq 0$, the over-strength ratios increase with the pile diameter and the steel ratio. For the cases with $P/(f_c'A_g)<0$, the over-strength ratios increase with the pile diameter, but decrease with the steel ratio.

Nonlinear Soil Springs

Based on the soil spring model described previously, this study adopts SPT-N values of 5, 10, 20, and 30 to change the characteristics of the soil springs. Fig. 8 presents the *p-y* curves for *D*=1m at SPT-N=5, 10, 20, and 30. It can be seen that the yield and ultimate displacements are 0.01m and 0.1m, respectively. The higher SPT-N value implies a stiffer ground.

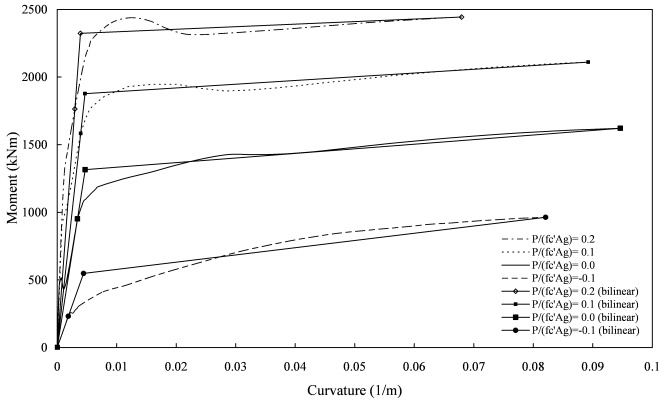

Fig. 5. Moment-curvature relationships for various axial force levels (D=1m and ρ_l=1%)

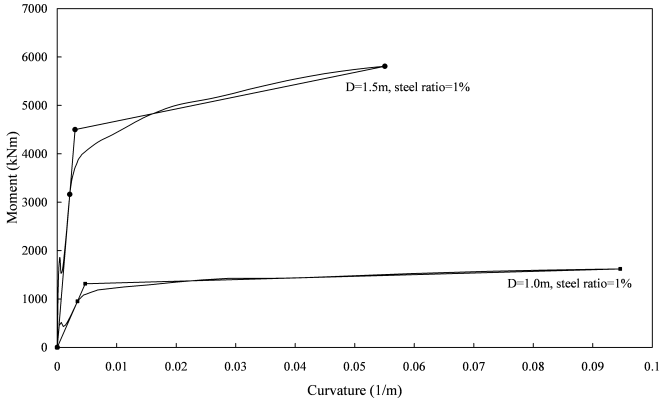

Fig. 6. Moment-curvature relationships for D=1.0 m and 1.5m ($P/(f_c'A_g)$=0 and ρ_l=1%)

PUSHEROVER CURVES AND DISPLACEMENT DUCTILITY CAPACITIES

The 64 sets of pushover analyses were conducted to obtain the pile-head load-deflection curves (pushover curves) by using SAP 2000 (2002).

Here, define the displacement ductility capacity as follows:

$$\psi = U_u / U_y \quad (6)$$

where U_u is the ultimate displacement, and U_y is the yield displacement.

On the influence of the axial force level, Fig. 9 compares the pushover curves for different axial force levels (*D*=1m, ρ_l=1% and in the soil stratum of SPT-N=5). It can be seen that both the yield load and the yield displacement increase with the axial force level because the pile section subjected to the high axial force level has higher sectional stiffness. However, the ultimate displacement decreases with the axial force level. The ultimate load is not necessarily larger for the section at the higher axial force level because the over-strength ratio for the section is low, and as a result a smaller post-yield displacement is enough to reach the ultimate moment.

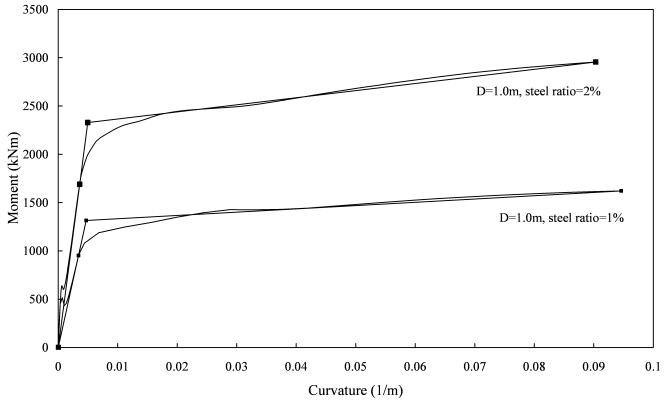

Fig. 7. Moment-curvature relationships for ρ_l=1% and 2% ($P/(f_c'A_g)$=0 and D=1m)

The curvature ductility, the sectional over-strength ratios, and the displacement ductility capacity for the above four cases (μ_ϕ, ω, ψ) values are denoted in Fig. 9. It can be seen that the ψ values do not consistently increase with the μ_ϕ values. However, the ψ values do consistently increase with the ω values.

On the influence of the pile diameter, Fig. 10 illustrates the pushover curves for *D*=1m and *D*=1.5m (ρ_l=1% and in the stratum of SPT-N=5). The larger pile-diameter gives the stiffer pushover curve with the larger yield and ultimate displacements. The displacement ductility capacity increases with the over-strength ratio, but decreases with the curvature ductility capacity. Although the curvature ductility capacity of *D*=1.5m is smaller than that of *D*=1m, the pile-head moment reaches its ultimate moment at a larger displacement due to the larger over-strength ratio.

On the influence of the longitudinal steel, Fig. 11 displays the pushover curves for ρ_l=1% and ρ_l=2% (*D*=1m and in the stratum of SPT-N=5. When the steel ratio increases, the curve becomes stiffer and exhibits the larger yield and ultimate displacements. The displacement ductility capacity also increases with the over-strength ratio, but decreases with the curvature ductility capacity.

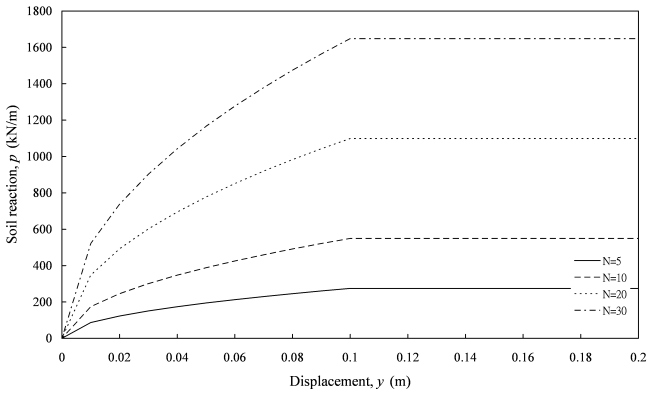

Fig. 8. P-y curves for D=1.0m

From the above comparisons, it can be noted that the curvature ductility capacity does not absolutely affect the displacement ductility capacity; by contrast, the sectional over-strength ratio plays a more prominent role in the displacement ductility capacity of the pile.

For the influence of the SPT-N value of the soil stratum, Fig. 12 shows the pushover curves for the pile ($P/(f_c'A_g)$=0, D=1m, and ρ_l=1%) in the stratum with the different SPT-N values. It can be observed that the pushover curve in the soil stratum with the higher SPT-N value is stiffer, and thus its yield and ultimate displacements are smaller. The stratum with the lower SPT-N gives the higher displacement ductility capacity; however, the values of those capacities are close.

DISCUSSIONS

Figure 13 collects the displacement ductility capacities of all the analysis cases with the corresponding sectional over-strength ratios. The displacement ductility capacity increases with the sectional over-strength ratio, and the correlation is good. For a specified over-strength ratio, the scatters among the displacement ductility capacities are due to the variation of the SPT-N values, and the lower capacity is for the stiffer ground. In Fig. 13, the data points with ω smaller than 1.4 are from the cases with $P/(f_c'A_g)\leq 0$, and those with ω larger than 1.4 are from the cases with the tensile axial forces. The variation range of the displacement ductility capacity at the smaller over-strength ratio is very small. It implies that the influence of soil stiffness is insignificant when the sectional over-strength ratio of a pile is low.

In Fig. 13, for the cases of the over-strength ratio above 1.6, the increment in the displacement ductility capacity notably increases. This is because the in-ground plastic zone is developing so that the pile displaces more. Generally, a fixed-head pile under lateral loads has two possible plastic zones. The first plastic zone is at the pile head which usually forms in the early stage of loadings. The second one occurs below the ground which forms after the formation of the pile-head plastic zone. The second plastic zone does not always occur, which depends on the value of the sectional over-strength ratio. With a lower value of over-strength ratio, the pile-head moment may reach its ultimate value before the formation of the in-ground plastic zone. For easy inspection and repair for piles after an earthquake, the in-ground plastic zone is normally not allowed in design. Under this consideration, the ultimate displacements for those analysis cases where the in-ground plastic zones have been developed in Fig. 13 should be re-defined as the displacements where the in-ground plastic zone just starts to form from a practical point of view. The displacement ductility capacities for these cases are therefore re-computed as plotted in hollow square points in Fig. 14. With this additional restriction, the displacement ductility capacity values will be reduced and seem saturated at a value between 4.4 and 5.5. Therefore, the displacement ductility capacity for fixed-head piles shall be further limited below 5 in engineering design to prevent the in-ground plasticity from occurring. The relationship between ψ and ω can be simply expressed as:

$$\psi = 1 + 6.8(\omega - 1) \leq 4.4 \tag{7}$$

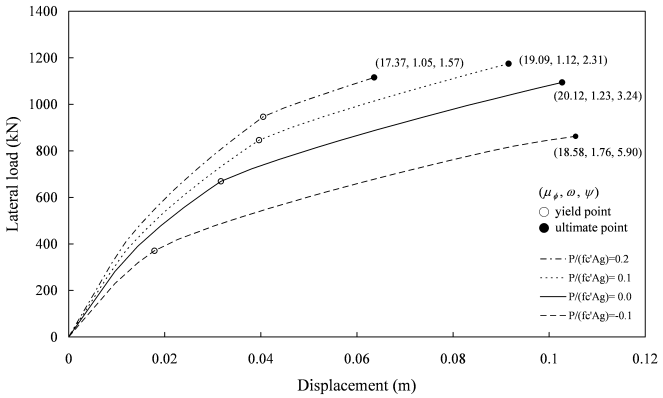

Fig. 9. Pushover curves for different axial force levels (D=1m, ρ_l=1%, SPT-N=5)

CONCLUSIONS

As compared to the curvature ductility capacity, the sectional over-strength ratio is important for the displacement ductility capacity of a fixed-head pile. The displacement ductility capacity of the pile increases with the over-strength ratio of the pile section. The influence of soil stiffness is less significant, especially when the sectional over-strength ratio of the pile is very low. Therefore, to enhance the ductility capacity of the pile, it is effective to increase the over-strength ratio of the pile section. On the other hand, the upper bound of displacement ductility capacity should be set to prevent the pile from developing the in-ground plasticity.

REFERENCES

Architecture Institute of Japan. [1988]. Recommendation for the design of building foundations. (in Japanese)

Budek A.M., Pristley, M.J.N., and Benzoni, G. [2000]. "Inelastic seismic response of bridge drilled-shaft RC pile/columns." Journal of Structural Engineering, 126, No. 4, pp. 510-517.

Chai, Y. H. [2002]. "Flexural strength and ductility of extended pile-shafts. I: Analytical model." Journal of Structural Engineering, 128, No. 5, pp. 586-594.

Chiou, J.S., Yang, H.H., and Chen, C.H. [2009], "Use of plastic hinge model in nonlinear pushover analysis of a pile," Journal of Geotechnical and Geoenviromental Engineeering, 135, No. 9, 1341-1346.

Kowalsky, M.J. (2000). "Deformation limit states for circular reinforced concrete bridge columns." Journal of Structural Engineering, 126, No. 8, pp. 869-878.

Mander, J.B., Priestley, M.J.N., and Park, R. [1988]. "Theoretical stress-strain model for confined concrete." Journal of the Structural Division (ASCE), 114, No. 8, pp. 1804-1826.

Song S.T., Chai, Y. H., and Hale, T. H. [2005]. "Analytical model for ductility assessment of fixed-head concrete piles." Journal of Structural Engineering, 131, No. 7, pp. 1051-1059.

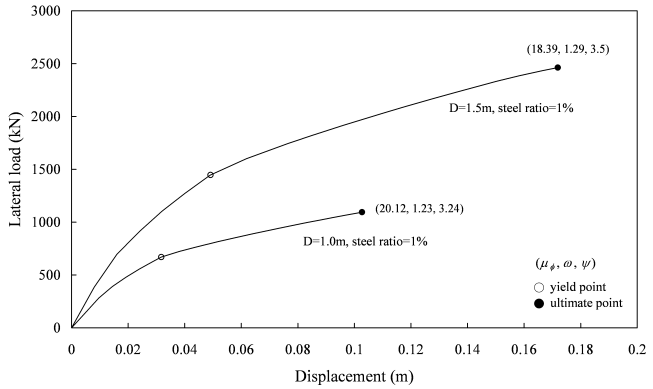

Fig. 10. Pushover curves for D=1.0m and 1.5m ($P/(f_c'A_g)=0$, $\rho_l=1\%$, SPT-N=5)

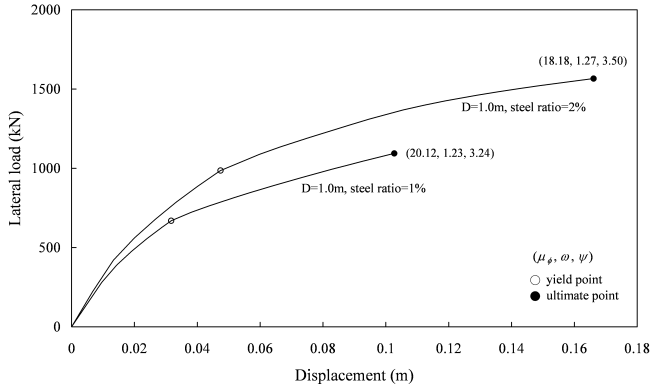

Fig. 11. Pushover curves for ρ_l of 1% and 2% ($P/(f_c'A_g)=0$, D=1m, SPT-N=5)

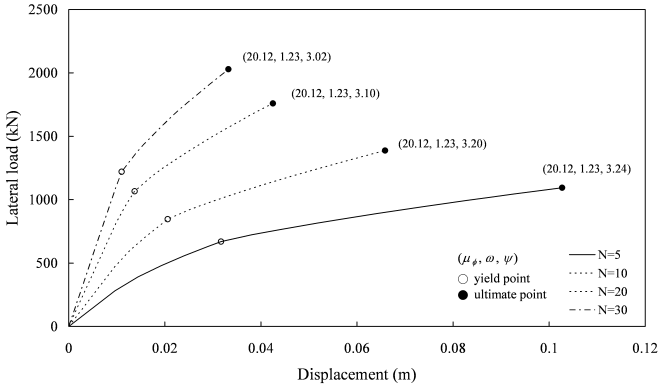

Fig. 12. Pushover curves for different SPT-N values ($P/(f_c'A_g)=0$, D=1m and $\rho_l=1\%$)

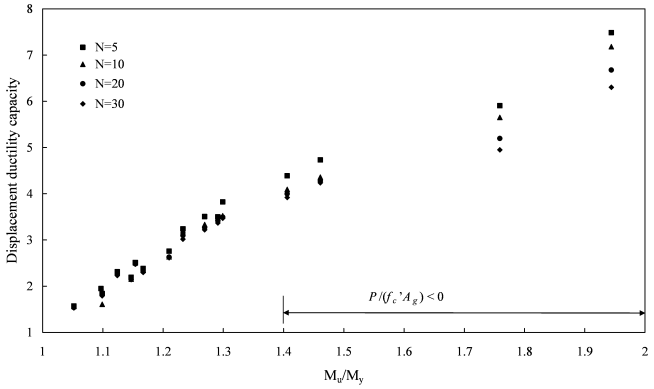

Fig. 13. Relationship of ψ versus ω

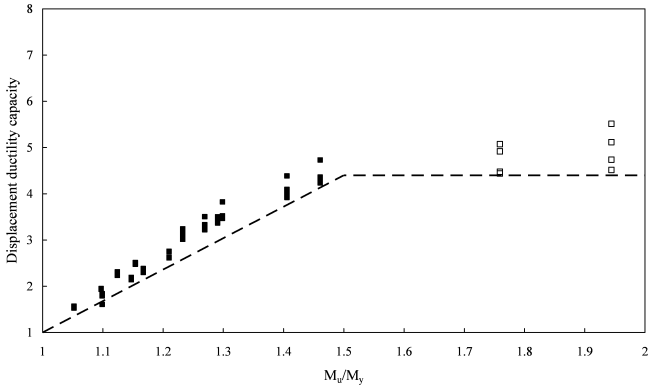

Fig. 14. Simplified relation of ψ versus ω